

PAPER • OPEN ACCESS

Searching for Dark Matter with the PADME experiment

To cite this article: Isabella Oceano and the PADME collaboration 2021 *J. Phys.: Conf. Ser.* **2156** 012058

View the [article online](#) for updates and enhancements.

You may also like

- [Search for light dark matter in the NA64 experiment](#)
S N Gninenko, N V Krasnikov and V A Matveev
- [A diamond active target for the PADME experiment](#)
G. Chiodini
- [The physics program of the PADME experiment](#)
A P Caricato, M Martino, I Oceano et al.

Searching for Dark Matter with the PADME experiment

Isabella Oceano, on behalf of PADME collaboration ¹.

Università del Salento, INFN Lecce

E-mail: isabella.oceano@le.infn.it

Abstract. The great success of the Standard Model has reached its maximum with the Higgs boson discovery. However, several anomalies observed in the universe when applying the gravitational theory, lead to believe that the visible matter is not the only constituent of the universe. A new matter component, called dark matter, must be introduced through an extension of the Standard Model. A simple scenario consisting in adding a new gauge symmetry $U_D(1)$ and, as a consequence, a new (massive) gauge boson, the dark photon A' . PADME is a new experiment of the Laboratori Nazionali di Frascati searching for the A' , decaying invisibly, produced in the fixed target annihilation $e^+e^- \rightarrow \gamma A'$. The technique used by the experiment to probe the dark photon hypothesis is the missing mass method. The PADME experiment took data in two runs. Some preliminary highlights from the ongoing data analysis effort are presented.

1. The dark photon

The theoretically best motivated Dark Matter (DM) candidates are Weakly Interacting Massive Particles (WIMPs), with mass of the order of $\sim 10^2$ GeV, interacting weakly and gravitationally with the known matter. Despite the popularity of this hypothesis, severe constraints have been put experimentally on this model [1]. This motivates the search of lighter dark matter candidates predicted by new models. One of the most interesting of them introduces a new gauge symmetry $U_D(1)$ representing a sector of new particles not directly interacting with the ordinary Standard Model (SM) particles. The corresponding new gauge boson A' might play the role of a neutral vector portal connecting the visible and the dark sector. Indeed, it can interact weakly with the SM particles thorough the kinetic mixing with the SM photon field described by the Lagrangian

¹ A.P. Caricato, M. Martino, I. Oceano, F. Oliva, S. Spagnolo (INFN Lecce and Dip. di Matematica e Fisica), G. Chiodini (INFN Lecce), F. Bossi, B. Buonomo, R. De Sangro, C. Di Giulio, D. Domenici, G. Finocchiaro, L.G. Foggetta, M. Garattini, A. Ghigo, F. Giacchino, P. Gianotti, I. Sarra, B. Sciascia, T. Spadaro, E. Spiriti, C. Taruggi, E. Vilucchi (INFN Laboratori Nazionali di Frascati), V. Kozhuharov (University of Sofia “St. Kl. Ohridski” and INFN Laboratori Nazionali di Frascati), G. Georgiev, S. Ivanov, R. Simeonov (University of Sofia “St. Kl. Ohridski”), F. Ferrarotto, E. Leonardi, F. Safai Tehrani, P. Valente (INFN Roma1), E. Long, G.C. Organtini, G. Piperno, M. Raggi (INFN Roma1 and Dip. di Fisica, “Sapienza” Università di Roma), S. Fiore (ENEA centro ricerche Frascati and INFN Roma1), V. Capirossi, F. Iazzi, F. Pinna (Politecnico di Torino), B. Liberti (Dip. di Fisica, Università di Roma “Tor Vergata”, INFN Laboratori Nazionali di Frascati), M. Martini (Università G. Marconi and INFN Laboratori Nazionali di Frascati), J. Alexander, A. Frankenthal (Dep. of Physics Cornell University).



term:

$$L_{int} = \frac{\epsilon}{2} F_{\mu\nu}^D F_{SM}^{\mu\nu} \quad (1)$$

where ϵ is an effective coupling parameter that can be as small as to preclude the discovery of the dark photon in many of the experiments. Besides ϵ , the only parameter of this model is the mass of the dark photon $m_{A'}$. The decay mode of the new particle depends on the mass hierarchy of the dark sector: if $m_{A'} > 2m_{DM}$, where m_{DM} is the mass of a hypothetical particle of dark sector, it will decay in dark particles, resulting in the so-called invisible decay channel, otherwise being the lightest dark sector particle, it will decay in SM particles, i.e. in visible decay channels.

2. PADME at Laboratori Nazionali di Frascati

The PADME experiment is designed to probe the dark photon hypothesis in the invisible decay channel. Its production happens in the annihilation $e^+e^- \rightarrow \gamma A'$, and its detection is possible by studying the missing mass $M_{miss}^2 = (p_{e^+} + p_{e^-} - p_\gamma)^2$, measured using the 4-momenta of the SM particles involved in the process. The LINAC of DAΦNE [2] provides a positron beam with a maximum energy $E_{e^+} \leq 550$ MeV. Therefore, the value of $m_{A'}$ that PADME can reach is limited to $m_{A'} \leq \sqrt{2m_e E_{e^+}} = 23.7$ MeV. A schematic picture of the experiment is reported in Figure 1. The beam hits an active target, made of CVD Diamond [3] [4], followed by a region where the particles propagate inside a vacuum chamber placed in the gap of a magnetic dipole. The photons produced in the interactions are detected by the calorimeter system, consisting of the main calorimeter (ECAL) [5] and the Small Angle Calorimeter (SAC) [6]. The first consists of 616 BGO crystals arranged in a cylindrical matrix with a central hole. Its main purpose is to detect the ordinary photon produced in association with the A' . A fast small angle calorimeter (SAC) is installed behind the central hole of ECAL. It consists of a 5×5 matrix of PbF_2 Cherenkov crystals and provides fast detection and rejection of forward photons from Bremsstrahlung of the positron beam on the target. To reject background processes with charged particles, a veto system is located inside the PADME vacuum vessel consisting of three stations of plastics scintillators (e^- veto, e^+ veto, high energy e^+ veto) [7].

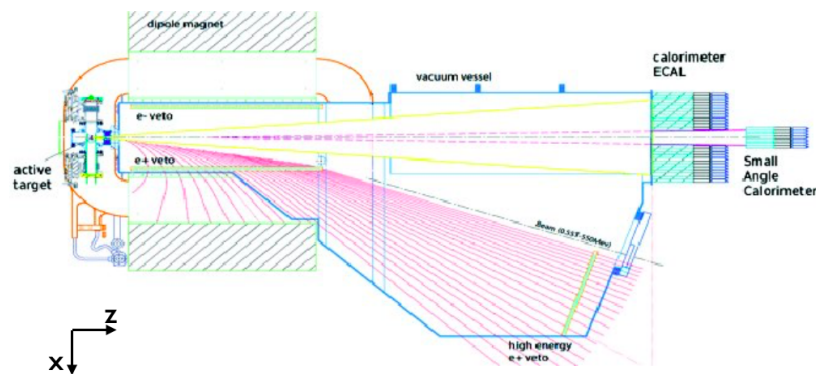


Figure 1. Layout of the PADME experiment (top view).

3. PADME data taking

The LINAC can provide PADME with two beam types: primary positrons and secondary positrons. The difference lies in the position along the beam line of the target used to convert

electrons to positrons. For the production of the secondary beam a $1.7 X_0$ Cu target, close to the PADME hall, is used. In case of the primary beam the conversion of the electrons happens in a $2 X_0$ W-Re target located at the beginning of the LINAC. PADME was built in July 2018 and it started taking data in September 2018 (RunI) employing alternatively secondary and primary positron beams. During RunI, the level of the beam induced background was higher than expected. Monte Carlo (MC) simulations, describing the complete beam line, showed that the beam related background was dominantly produced in the Be window separating the LINAC from the PADME vacuum. Dedicated studies based on these simulations helped the LINAC staff to plan improvements of the beam transport thus achieving a significant reduction of the beam related background in the RunII which took place from September 2020 to December 2020. For limiting the pile-up probability, the positron density has been limited to ~ 100 particles/ns, extending as much as possible the beam pulse length [8]. Figure 2 shows the total photon energy measured by the ECAL detector for three different beam configurations: RunI with secondary beam (red dots), RunI with primary beam (blue dots) and RunII with primary beam (green dots). The beam induced background decreases a lot using the primary beam. Indeed, with

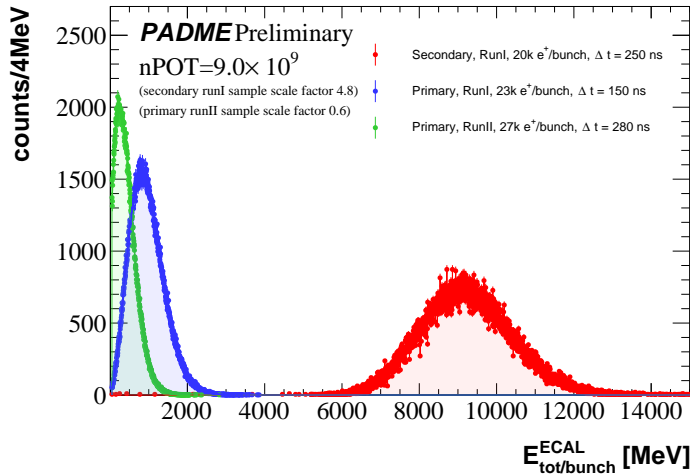


Figure 2. Total energy per bunch in the ECAL detector in the three different data taking conditions: RunI and secondary positron beam (red distribution), RunI and primary positron beam (blue distribution), RunII and primary positron beam (green distribution).

the secondary beam, the experiment was overwhelmed by secondary particles from the shower produced in the conversion occurring too close to the PADME hall and leading to a background level in ECAL of 0.551 ± 0.073 MeV/ e^+ . This was reduced down to 0.037 ± 0.019 MeV/ e^+ with the primary beam and, after the beam line optimisation for RunII, it was further reduced down to 0.0027 ± 0.0130 MeV/ e^+ (the errors are the width of the gaussian fits to the distributions).

4. Background processes in PADME

The most dangerous background comes from Bremsstrahlung photons, due to the high cross section of the process and to the presence of a single photon in the electromagnetic calorimeter that can mimic the signal. The Bremsstrahlung cross section is $\sigma(e^+N \rightarrow e^+N\gamma) \sim 4$ b for a beam energy $E_{beam} = 550$ MeV. Since Bremsstrahlung photons are emitted in the forward direction, PADME is expected to detect all this radiation, with a geometrical acceptance very close to 1, with most of the photons hitting the SAC. The correlation between the energy of the photon detected in the SAC and the e^+ veto channel hit by a positron (related to the positron kinetic energy) in time coincidence $|\Delta t| = |t_\gamma - t_{e^+}| < 1$ ns is shown in Figure 3 for data collected during RunII ($E_{beam} = 430$ MeV, $N_{e^+/\text{bunch}} = 27 \times 10^3$ and bunch length of 280 ns). The Figure 3 shows that in RunII the time coincidence is enough to select a clear sample of Bremsstrahlung interactions. The other SM process that can be a background for the dark photon search is the

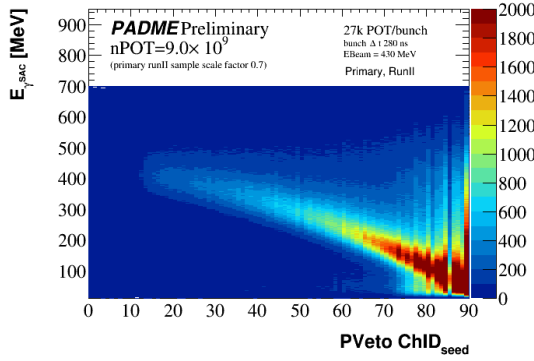


Figure 3. SAC cluster energy as a function of e^+ veto channel number of a cluster in time for data collected with primary beam in RunII.

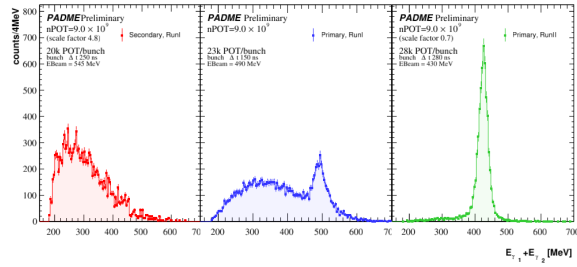


Figure 4. Distribution of the energy sum of two photons events with loose annihilation selection cuts for the three different data taking conditions: in red data collected in RunI with secondary beam, in blue in RunI with primary beam and in green in RunII with primary beam.

annihilation $e^+e^- \rightarrow \gamma\gamma$ if one of the two photons is undetected. At leading order the cross section is $\sigma(e^+e^- \rightarrow \gamma\gamma) = 1.55 \text{ mb}$ for $E_{beam} = 550 \text{ MeV}$. This process is used also as candle for the experiment. The ECAL detector was used to study the annihilation in two photons. The events selection was based on the request of time coincidence $|\Delta t| = |t_{\gamma_1} - t_{\gamma_2}| < 10 \text{ ns}$ between the two photons, with the most energetic one inside a radial fiducial region $R_\gamma \in [116, 258] \text{ mm}$. The sum of the energy of the two photons for events passing the selection is reported in Figure 4 for the three different beam configurations: in red the distribution for RunI with secondary beam, in blue for RunI with primary beam and in green for RunII. From the comparison, the great improvement in event reconstruction, due to the beam background reduction, clearly emerges.

5. PADME challenges

The need for high efficiency in background rejection motivates an intense work in the optimisation of the reconstruction of the signals collected using the e^+ veto and ECAL detectors. For the first detector, an important improvement was obtained with a fine tuning of the calibration as a spectrometer, for the latter a significant effort was put to disentangle multiple hits in the same digitised waveform of a single BGO crystal.

5.1. Charged particle veto as a spectrometer

In PADME a charged particle emerging from the target enters in a region with a uniform magnetic field and it is horizontally deflected: the positrons that do not lose energy in the interaction with the target are bent out of the experiment acceptance, while positrons that lose an energy $\geq 50 \text{ MeV}$ hits the positron veto in a z position corresponding to its momentum in the direction perpendicular to the magnetic field. In ideal conditions:

$$p(z) = \frac{0.3B[(z - z_c)^2 + x^2]}{2x} \quad (2)$$

where B is the magnetic field in Tesla, z_c is the z coordinate in mm in where the magnetic field is setted on and x is the distance in mm of the e^+ veto along the x axis. A MC simulation of single positrons of different energies hitting the center of the Diamond target perpendicularly was used to extract the z position of the e^+ veto hit as a function of the energy. In the simulation the magnetic field was described in details, including the map of the fringe field and the weak dependence on x of the intensity.

5.2. ECAL Multi-hit reconstruction

High efficiency for photon reconstruction in ECAL is mandatory for the PADME experiment. Due to the slow BGO scintillation decay time, it is possible to have more than one hit in the digitised waveform. An algorithm was developed to identify multiple hits by fitting the waveform with several single hit template curves extracted from data. After reconstructing a special run with a poissonian $1e^+$ per bunch, the total cluster energy distribution was well reproduced by a fit with several gaussian peaks (see Figure 5) with amplitudes consistent with the probability of n positrons (with $n= 1, \dots, 7$) for an average e^+ multiplicity, from the fit, equal to $N_{e^+} = 1.18 \pm 0.22$.

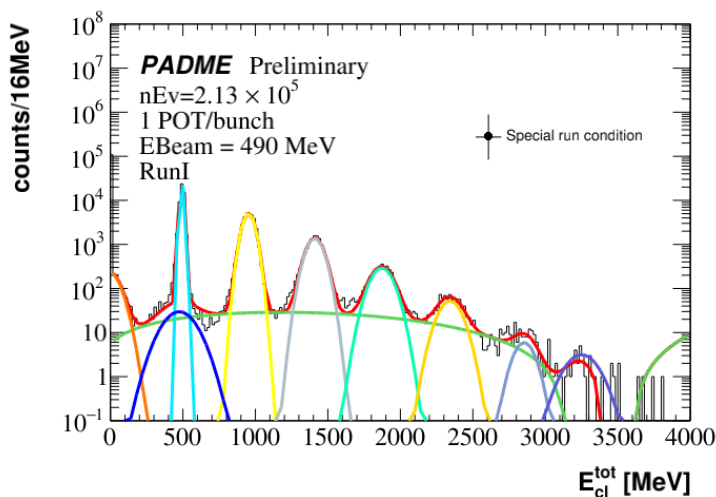


Figure 5. Total cluster energy of the ECAL detector hit by beam bunches with an average multiplicity of one positron.

6. Conclusion

The PADME experiment uses for the first time a positron beam to search for a dark photon signal produced in the annihilation with the electron of a fixed target. In this search the missing mass technique is employed. During PADME RunI and RunII all detectors of the experiment performed according to the design expectation. The MC simulation helped the understanding of the beam induced background suggesting interventions that lead to a significant background reduction in RunII. The resulting improvement in the reconstruction and identification of SM physics processes, such as Bremsstrahlung and two photons annihilation is clearly seen.

References

- [1] P. Cushman, et al, *Snowmass cf1 summary: Wimp dark matter direct detection*, arXiv:1310.8327 (2013).
- [2] P. Valente et al., *Linear Accelerator Test Facility at LNF Conceptual Design Report*, arXiv:1603.05651 (2016).
- [3] F. Oliva , *Operation and performance of the active target of PADME*, Nuclear Inst. and Methods in Physics Research, A 162354, <https://doi.org/10.1016/j.nima.2019.162354> (2019).
- [4] I. Oceano , *The performance of the diamond active target of the PADME experiment*, Journal of Instrumentation 15 C04045 (2020).
- [5] G. Piperno et al., *Characterisation and performance of the PADME electromagnetic calorimeter*, Journal of Instrumentation, vol. 15 (2020).
- [6] A. Frankenthal et al., *Characterization and performance of PADME's Cherenkov-based small-angle calorimeter*, Nuclear Instruments and Methods in Physics Research, vol. 919 (2019).
- [7] G. Georgiev et al., *The PADME tracking system*, RAD Association Journal, DOI:10.21175/radj.2016.03.034 (2016).
- [8] Y M Zhang et al., *Research of L-band disk-loaded waveguides travelling wave accelerating structures for a high power Linac*, IOP Publishing, Vol.874, DOI:10.1088/1742-6596/874/1/012018 (2017).
- [9] M. Tanabashi et al., *Review of particle physics. Phys. Rev. D*, 98:030001 (2018).